ISSN: 0067-2904

Impact of Heat Transfer and Inclined MHD on A Non-Uniform Inclined Asymmetrical Channel with Couple Stress Fluid Through A Porous Medium

Hanaa Abdulhussein[1*], Ahmed M. Abdulhadi [2]
[1] *Department of Science, College of Basic Education, Wasit University, AL Kut , Iraq*
[2] *Department of Mathematics, College of Science, University of Baghdad, Baghdad, Iraq*

Received: 14/3/2022 Accepted: 20/10/2022 Published: 30/9/2023

Abstract

The goal of this study is to investigate the effects of heat transfer on a non-uniform inclined asymmetrical channel with couple stress fluids via a porous medium using incline magnetohydrodynamics. The governing equation is studied while using low Reynolds approximations and long-wavelength assumptions. Mathematical expressions for (pressure gradient), (temperature), (axial velocity), (heat temperature coefficient), and (stream function). A precise set of values for the various parameters in the present model has been used. The mathematical expressions for axial velocity, stream function, pressure gradient, and pressure rise per wavelength have been derived analytically. "MATHEMATICA" is used to present the computational results in the form of graphs. It has been noticed that both the pressure rise and the pressure gradient decrease with the rise of the inclination magnetic field angle and Darcy number, while as the Grashof number increases, the pressure gradient reduces and the pressure also increases. According to this study, the heat transfer coefficient and temperature rise when the Brinkman number and the Hartman number are up. As the Hartman number and couple stress increase, the incidence of trapped boluses diminishes in size and vanishes in the direction downstream. The bolus size can also be increased by raising the non-uniform channel's Darcy number.

Keywords: "Non-uniform channel, Heat transfer, Inclined MHD, Couple-stress, Porous medium"

تأثير نقل الحرارة و MHD المائل على قناة غير متناظرة مائلة غير منتظمة مع سائل إجهاد ثنائي خلال وسط مسامي

هناء عبدالحسين* ، احمد مولود عبدالهادي
قسم العلوم ، كلية التربية الاساسية ، جامعة واسط ،الكوت ، العراق
قسم الرياضيات، كلية العلوم، جامعة بغداد، بغداد ، العراق

الخلاصة

الهدف من هذه الدراسة هو التحقيق في آثار انتقال الحرارة على قناة غير متناظرة مائلة غير منتظمة مع سائل اجهاد ثنائي عبر وسط مسامي باستخدام الهيدروديناميكية المغناطيسية المائلة. تمت دراسة المعادلة الحاكمة أثناء استخدام تقديرات رينولدز المنخفضة وافتراضات الطول الموجي الطويل. التعبيرات الرياضية لـ (تدرج الضغط) و (درجة الحرارة) و (السرعة المحورية) و (معامل انتقال الحرارة) و (دالة التدفق). تم استخدام مجموعة

*Email: hshatty@uowasit.edu.iq

دقيقة من القيم للمعلمات المختلفة في النموذج الحالي. تم اشتقاق التعبيرات الرياضية للسرعة المحورية، ودالة التدفق، وتدرج الضغط، وارتفاع الضغط لكل طول موجة بشكل تحليلي. يتم استخدام "MATHEMATICA" لتقديم النتائج الحسابية في شكل رسوم بيانية. لوحظ أن كلا من ارتفاع الضغط وتدرج الضغط ينخفضان مع ارتفاع زاوية ميل المجال المغناطيسي ورقم دارسي، بينما يزداد رقم جراشوف ينخفض تدرج الضغط ويزداد ارتفاع الضغط. وفقًا لهذه الدراسة، يرتفع معامل انتقال الحرارة ودرجة الحرارة عندما يرتفع كل من رقم برينكمان ورقم هارتمان. مع زيادة عدد هارتمان وإجهاد الثنائي، يتضاءل حجم بلعات المحاصرة ويختفي في اتجاه مجرى المصب. يمكن أيضًا زيادة حجم البلعة عن طريق رفع رقم دارسي للقناة غير المنتظمة.

1. Introduction

One of the most well-known physiological processes is called peristalsis, and it is responsible for mixing and transferring the fluids in a distensible tube by diminishing and expanding the area in a series of waves. The neuromuscular properties of any tubular smooth muscle structure are primarily responsible for this phenomenon. It is a wave-like motion with a set speed and wavelength in this muscular tube wall. This process uses urine transport from the kidney to the bladder, bile from the gallbladder to the duodenum, spermatozoa in the male reproductive tract's efferent ducts, the fallopian tubes, and blood flow via microscopic blood vessels. Many biomedical devices, such as dialysis machines, heart-lung machines, and blood pump machines, use this mechanism. The roller and finger pumps are also used with the same mechanism. because of its ability to explain biologically complicated fluids like liquid crystals and human blood. Study of a couple stress fluid is extremely valuable in comprehending many physical difficulties. Non-Newtonian fluids, such as couple stress fluids, are those in which particle size is taken into account. Peristaltic transfer of MHD has recently been studied by [1–3]. They have conducted some recent investigations into the peristaltic transport of couple stress fluid [4–8]. Blood was used as a couple stress fluid in other researches, which used no-slip conditions, despite the fact that in actual systems. Some slips were usually presented. It is surprising how little research has been done on the subject of peristalsis and heat transmission. While blood is taken out of the body, the thermodynamic features of the blood become more relevant than the blood inside the body. With understanding that heat transmission is critical to the movement of blood in tubes. Shit and Ranjit [9] studied the fluid's peristalsis in non-uniform and asymmetric channels when an external magnetic field is provided. Salman and Abdulhadi [10] studied the peristalsis of pseudoplastic nanofluid through a porous medium with coupling stress in an inclined tapered asymmetric channel. Ramesh [11] studied how heat and mass transfer are affected by magnetohydrodynamic coupling stress in an inclined asymmetric channel. Hayat *et al*.[12] investigated the effect of variable viscosity on tangent hyperbolic fluid peristaltic transport with heat and mass transfer. Salman and Ali [13] studied a two-dimensional asymmetric, tapered channel with an MHD non-Newtonian Jeffery fluid flowing through the porous media and heat transfer. This paper is an illustration of a model for the blood flow in living organisms. With the help of incline magnetohydrodynamics, the mathematical model of the impact of couple stress fluid and heat transfer in non-uniform and asymmetric channels via a porous medium is established. The governing equation is studied while using low Reynolds approximations and long-wavelength assumptions. For fluid flow, essential variables are studied and their effects are depicted using graphs.

2. Formulation and solution of mathematical problems

An incompressible couple-stress fluid and heat transfer via a Non-uniform channel and an inclined asymmetry with a porous medium may be considered in the middle of the action of the magnetic field. Waves with variable amplitudes and phases, but at a constant c, propagate along the channel walls. See Figure 1.

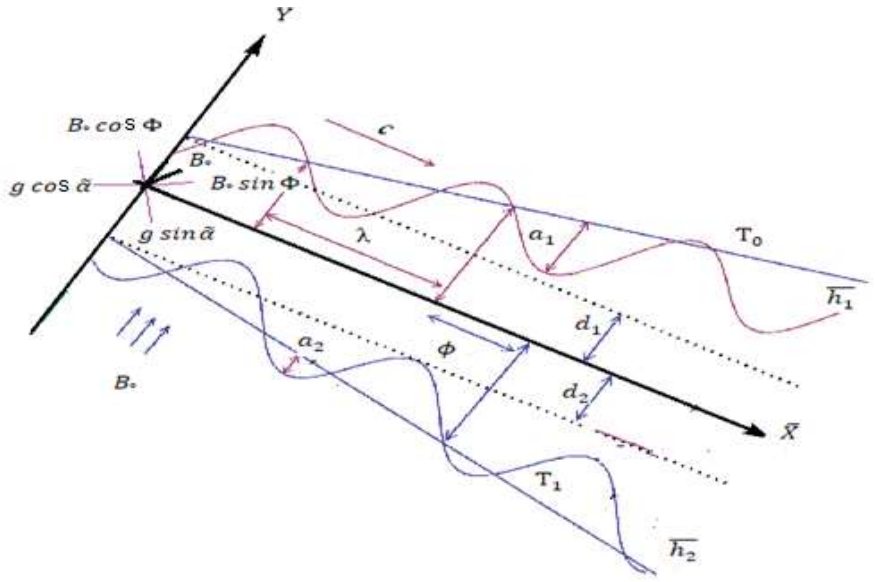

Figure 1: Geometry graph of the problem.

Impose $\bar{Y} = \overline{h_1}\ (\bar{X}, \bar{t})$ and $\bar{Y} = \overline{h_2}\ (\bar{X}, \bar{t})$ represent the channel's upper and bottom walls, respectively, so that

$$(\bar{X}, \bar{t}) = d_1 + (\bar{X} - c\bar{t}) \tan\tilde{\alpha} + a_1 \cos\left[\frac{2\pi}{\lambda}(\bar{X} - c\bar{t})\right]\overline{h_1} \quad \text{upper wall} \quad (1)$$

$$(\bar{X}, \bar{t})\overline{h_2} = -d_2 - (\bar{X} - c\bar{t}) \tan\tilde{\alpha} - a_2 \cos\left[\frac{2\pi}{\lambda}(\bar{X} - c\bar{t}) + \phi\right] \quad \text{bottom wall} \quad (2)$$

where $a_1 and\ a_2$ are the amplitudes of waves λ is wavelength, $\bar{t}$ is the time , c is wave speed , ϕ $(0 \le \phi \le \pi)$ the phase difference between the walls of the channel the rectangular Cartesian coordinates are used $\bar{X}$and $\bar{Y}$. The channel's axis is measured by $\bar{X}$, and the transverse axis is measured by $\bar{Y}$, which is perpendicular to $\bar{X}$. The heights of the upper and bottom walls of the channel from the central line are denoted by $d_1, and\ d_2$. width of the channel wells inclination with respect to the central axis- $\bar{X}$. It is worth noting that $\phi = 0$ corresponds to an asymmetry with out-of-phase waves, whereas $\phi = \pi$ relates to waves that are in phase. Furthermore, $a_1, a_2, d_1, d_2$and ϕ meet the criteria
$a_1^2 + a_2^2 + 2a_1a_2cos\phi \le (d_1 + d_2)^2$.

The governing equations for unsteady flow in incompressible couple stress of an asymmetric with the inclination of the magnetic field via porous medium in terms of continuity, motion and energy equations.

$$\frac{\partial \bar{\mathrm{U}}}{\partial \bar{\mathrm{X}}} + \frac{\partial \bar{\mathrm{V}}}{\partial \bar{\mathrm{Y}}} = 0 \quad (3)$$

$$\rho\left(\frac{\partial \bar{\mathrm{U}}}{\partial \bar{t}} + \bar{\mathrm{U}}\frac{\partial \bar{\mathrm{U}}}{\partial \bar{X}} + \bar{\mathrm{V}}\frac{\partial \bar{\mathrm{U}}}{\partial \bar{Y}}\right) = -\frac{\partial \bar{\mathrm{P}}}{\partial \bar{\mathrm{X}}} + \mu\nabla^2\bar{U} - \eta\nabla^4\bar{U} - \tilde{\sigma}B_\circ^2\, cos\,\Phi\,(\bar{\mathrm{U}}\, cos\,\Phi - \bar{\mathrm{V}}\, sin\,\Phi) - \frac{\mu}{k_\circ}\bar{\mathrm{U}} + \rho g\dot{\alpha}\,(\mathrm{T} - \mathrm{T}_\circ) sin\tilde{\alpha} + \rho g sin\tilde{\alpha} \quad (4)$$

$$\rho\left(\frac{\partial \bar{\mathrm{V}}}{\partial \bar{t}} + \bar{\mathrm{U}}\frac{\partial \bar{\mathrm{V}}}{\partial \bar{\mathrm{X}}} + \bar{\mathrm{V}}\frac{\partial \bar{\mathrm{V}}}{\partial \bar{\mathrm{Y}}}\right) = -\frac{\partial \bar{\mathrm{P}}}{\partial \bar{\mathrm{Y}}} + \mu\nabla^2\bar{\mathrm{V}} - \eta\nabla^4\bar{\mathrm{V}} + \tilde{\sigma}B_\circ^2\, sin\,\Phi\,(\bar{\mathrm{U}}\, cos\,\Phi - \bar{\mathrm{V}}\, sin\,\Phi) - \frac{\mu}{k_\circ}\bar{\mathrm{V}} - \rho g cos\tilde{\alpha} \quad (5)$$

$$\rho C_p\left(\frac{\partial \mathrm{T}}{\partial \bar{t}}+\bar{\mathrm{U}}\frac{\partial \mathrm{T}}{\partial \bar{\mathrm{X}}}+\bar{\mathrm{V}}\frac{\partial \mathrm{T}}{\partial \bar{Y}}\right)=\widetilde{\mathrm{K}}\left(\frac{\partial^2 \mathrm{T}}{\partial \bar{\mathrm{X}}^2}+\frac{\partial^2 \mathrm{T}}{\partial \bar{Y}^2}\right)+\mu\left[2\left\{\left(\frac{\partial \bar{\mathrm{U}}}{\partial \bar{\mathrm{X}}}\right)^2+\left(\frac{\partial \bar{\mathrm{V}}}{\partial \bar{\mathrm{Y}}}\right)^2\right\}+\left(\frac{\partial \bar{\mathrm{U}}}{\partial \bar{\mathrm{Y}}}+\frac{\partial \bar{\mathrm{V}}}{\partial \bar{\mathrm{X}}}\right)^2\right]+$$
$$\eta\left[\left(\frac{\partial^2 \bar{\mathrm{U}}}{\partial \bar{\mathrm{X}}^2}+\frac{\partial^2 \bar{\mathrm{U}}}{\partial \bar{\mathrm{Y}}^2}\right)^2+\left(\frac{\partial^2 \bar{\mathrm{V}}}{\partial \bar{\mathrm{X}}^2}+\frac{\partial^2 \bar{\mathrm{V}}}{\partial \bar{\mathrm{Y}}^2}\right)^2\right]+\tilde{\sigma}B_\circ^2(\bar{\mathrm{U}}\,cos\,\Phi-\bar{\mathrm{V}}\,sin\,\Phi)^2 \quad (6)$$

Where $\overline{V'}=(\bar{U},\bar{\mathrm{V}},0)$ is velocity vector, $\dot{\alpha}$ is coefficient of thermal expansion, $\bar{P}$ is the fluid pressure, ρ is density of fluid, Φ is inclination of the magnetic field angle, μ is dynamic viscosity, η is a constant linked to the couple stress, C_p is the specific heat at constant pressure. Impact$\overrightarrow{\mathrm{B}_\circ}=(B_\circ\,sin\,\Phi\,,B_\circ\,cos\,\Phi\,,0)$ the magnetic field vector $k_\circ$ is the permeability parameter,T is the temperature, g is the acceleration by gravity, $\tilde{\sigma}$ is the fluids electrical conductivity, $\widetilde{\mathrm{K}}$ is the thermal conductivity. The induced electric field is not taken into consideration at all, because a low magnetic Reynolds number is assumed. $\nabla^2=\frac{\partial^2}{\partial \bar{\mathrm{X}}^2}+\frac{\partial^2}{\partial \bar{\mathrm{Y}}^2}$, $\nabla^4=\frac{\partial^4}{\partial \bar{\mathrm{X}}^4}+2\frac{\partial^4}{\partial \bar{\mathrm{X}}^2\partial \bar{Y}^2}+\frac{\partial^4}{\partial \bar{Y}^4}$.

The fixed frame's$(\bar{X},\bar{Y})$ flow field and the wave frame's$(\grave{\mathrm{x}},\grave{\mathrm{y}})$ wave field are also considered the motions of an unsteady and steady-state. It is important to think about the relationship between the wave $(\grave{\mathrm{x}},\grave{\mathrm{y}})$ and the fixed frames $(\bar{X},\bar{Y})$ with a velocity of c as they move apart from one another as a result of the transformations below.

$$\grave{\mathrm{v}}\,(\grave{\mathrm{x}},\grave{\mathrm{y}})=\bar{V}\ ,\ \grave{\mathrm{y}}=\bar{Y}\ ,\mathrm{T}=\overline{\mathrm{T}}\ ,\ \grave{\mathrm{x}}=\bar{X}-c\bar{t},\grave{p}=\bar{P}\ ,\grave{\mathrm{u}}\,(\grave{\mathrm{x}},\grave{\mathrm{y}})=\bar{U}-c \quad (7)$$

In which (ù, v̀) and $(\bar{\mathrm{U}},\bar{\mathrm{V}})$ are the waves' and laboratories' velocities, respectively. The governing equations(3-6) are expressed in wave frame using the transformations mentioned above.

$$\frac{\partial \grave{\mathrm{u}}}{\partial \grave{\mathrm{x}}}+\frac{\partial \grave{\mathrm{v}}}{\partial \grave{\mathrm{y}}}=0 \quad (8)$$

$$\rho\left((\grave{\mathrm{u}}+c)\frac{\partial \grave{\mathrm{u}}}{\partial \grave{\mathrm{x}}}+\grave{\mathrm{v}}\frac{\partial \grave{\mathrm{u}}}{\partial \grave{\mathrm{y}}}\right)$$
$$=-\frac{\partial \grave{p}}{\partial \grave{\mathrm{x}}}+\mu\nabla^2\grave{\mathrm{u}}-\eta\nabla^4\grave{\mathrm{u}}-\tilde{\sigma}B_\circ^2\,cos\,\Phi\left((\grave{\mathrm{u}}+c)\,cos\,\Phi-\grave{\mathrm{v}}\,sin\,\Phi\right)$$
$$-\frac{\mu}{k_\circ}(\grave{\mathrm{u}}+c)\ +\rho g\dot{\alpha}\,(\overline{\mathrm{T}}-\mathrm{T}_\circ)sin\tilde{\alpha}+\ \rho g sin\tilde{\alpha} \quad (9)$$

$$\rho\left((\grave{\mathrm{u}}+c)\frac{\partial \grave{\mathrm{v}}}{\partial \grave{\mathrm{x}}}+\grave{\mathrm{v}}\frac{\partial \grave{\mathrm{v}}}{\partial \grave{\mathrm{y}}}\right)=-\frac{\partial \grave{p}}{\partial \grave{\mathrm{y}}}+\mu\nabla^2\grave{\mathrm{v}}-\eta\nabla^4\grave{\mathrm{v}}+\tilde{\sigma}B_\circ^2\,sin\,\Phi\,((\grave{\mathrm{u}}+c)\,cos\,\Phi-\grave{\mathrm{v}}\,sin\,\Phi)-$$
$$\frac{\mu}{k_\circ}\grave{\mathrm{v}}\ -\rho g cos\tilde{\alpha} \quad (10)$$

$$\rho C_p\left((\grave{\mathrm{u}}+c)\frac{\partial \overline{\mathrm{T}}}{\partial \grave{\mathrm{x}}}+\grave{\mathrm{v}}\frac{\partial \overline{\mathrm{T}}}{\partial \grave{\mathrm{y}}}\right)=\widetilde{K}\left(\frac{\partial^2 \overline{\mathrm{T}}}{\partial \grave{\mathrm{x}}^2}+\frac{\partial^2 \overline{\mathrm{T}}}{\partial \grave{\mathrm{y}}^2}\right)+\mu\left[2\left\{\left(\frac{\partial \grave{\mathrm{u}}}{\partial \grave{\mathrm{x}}}\right)^2+\left(\frac{\partial \grave{\mathrm{v}}}{\partial \grave{\mathrm{y}}}\right)^2\right\}+\left(\frac{\partial \grave{\mathrm{u}}}{\partial \grave{\mathrm{y}}}+\frac{\partial \grave{\mathrm{v}}}{\partial \grave{\mathrm{x}}}\right)^2\right]+\eta\left[\left(\frac{\partial^2 \grave{\mathrm{u}}}{\partial \grave{\mathrm{x}}^2}+\right.\right.$$
$$\left.\left.\frac{\partial^2 \grave{\mathrm{u}}}{\partial \mathrm{y}^2}\right)^2+\left(\frac{\partial^2 \grave{\mathrm{v}}}{\partial \grave{\mathrm{x}}^2}+\frac{\partial^2 \grave{\mathrm{v}}}{\partial \grave{\mathrm{y}}^2}\right)^2\right]+\tilde{\sigma}B_\circ^2\left((\grave{\mathrm{u}}+c)\,cos\,\Phi-\grave{\mathrm{v}}\,sin\,\Phi\right)^2 \quad (11)$$

To reduce the number of additional parameters, we shall define the following non-dimensional quantities:

$$y=\frac{\grave{\mathrm{y}}}{d_1},\ x=\frac{\grave{\mathrm{x}}}{\lambda},\ h_1(x)=\frac{\overline{h_1}\,(\bar{X})}{d_1},\ h_2(x)=\frac{\overline{h_2}\,(\bar{X})}{d_1},\ \theta=\frac{\overline{\mathrm{T}}-\mathrm{T}_0}{\mathrm{T}_1-\mathrm{T}_0},\ \mathrm{u}=\frac{\grave{\mathrm{u}}}{c},\ \mathrm{v}=\frac{\lambda\grave{\mathrm{v}}}{cd_1},\ \frac{d_1^2\,\grave{p}(\grave{x})}{\lambda\mu c}=p\ ,$$
$$t=\frac{c\bar{t}}{\lambda},\ R_e=\frac{c\rho d_1}{\mu},\ \delta=\frac{d_1}{\lambda},\ H=\mathrm{B}_o d_1\sqrt{\frac{\tilde{\sigma}}{\mu}},\ P_r=\frac{\mu\,C_p}{\widetilde{K}},\ \gamma=d_1\sqrt{\frac{\mu}{\eta}},\ D_a=\frac{k_o}{d_1^2},\ F_r=\frac{c^2}{g d_1}, \quad (12)$$
$$B_r=P_r.\,E_c\ ,G_r=\frac{\rho\,g(\mathrm{T}_1-\mathrm{T}_0)\,\dot{\alpha}\,d_1}{\mu\,c},\ E_c=\frac{c^2}{(\mathrm{T}_1-\mathrm{T}_0)\,C_p}.$$

where H is Hartmann number, R_e is Reynolds number, δ is Wave number, γ is Couple stress parameter, P_r is Prandtl number, D_a is Darcy number, F_r is Froude number, B_r is Brinkman number, E_c is Eckert number, and G_r is Grashof number.

$$h_1(x) = 1 + \left(\frac{\lambda \tan\tilde{\alpha}}{d_1}\right)x + \frac{a_1}{d_1}\cos(2\pi x) \quad (13)$$

$$h_2(x) = -\frac{d_2}{d_1} - \left(\frac{\lambda \tan\tilde{\alpha}}{d_1}\right)x - \frac{a_2}{d_1}\cos(2\pi x + \phi) \quad (14)$$

According to equations (13) and (14), the dimensionless shape of the peristaltic channel walls is shown in $h_1(x)$ and $h_2(x)$

$$h_1(x) = 1 + kx + a\cos(2\pi x) \quad (15)$$

$$h_2(x) = -d - kx - b\cos(2\pi x + \phi) \quad (16)$$

where $a = \frac{a_1}{d_1}, b = \frac{a_2}{d_1}, d = \frac{d_2}{d_1}, k = \left(\frac{\lambda \tan\tilde{\alpha}}{d_1}\right)$ is referred to as the channel's non-uniform parameter and ϕ the relation $a^2 + b^2 + 2ab\cos\phi \leq (1+d)^2$

where(ψ) is stream function of velocity components u and v that is dimensionless $u = \frac{\partial \psi}{\partial y}$ and $v = -\frac{\partial \psi}{\partial x}$, respectively, and satisfy the continuity equation (8).

In terms of stream function , the dimensionless variables are specified in equations (9-11) and translated into the following equations.

$$R_e.\delta\left[\left(\frac{\partial\psi}{\partial y}.\frac{\partial}{\partial x} - \frac{\partial\psi}{\partial x}.\frac{\partial}{\partial y}\right)\frac{\partial\psi}{\partial y} + \frac{\partial^2\psi}{\partial x\partial y}\right] = -\frac{\partial p}{\partial x} + \delta^2\frac{\partial^3\psi}{\partial x^2\partial y} + \frac{\partial^3\psi}{\partial y^3} - \frac{1}{\gamma^2}\left(\delta^4\frac{\partial^5\psi}{\partial x^4\partial y} + 2\delta^2\frac{\partial^5\psi}{\partial x^2\partial y^3} + \frac{\partial^5\psi}{\partial y^5}\right) - H^2\cos\Phi\left[\left(\frac{\partial\psi}{\partial y} + 1\right)\cos\Phi + \frac{\partial\psi}{\partial x}\,\delta\sin\Phi\right] - \frac{1}{D_a}\left(\frac{\partial\psi}{\partial y} + 1\right) + \frac{R_e}{F_r}\sin\tilde{\alpha} + G_r\,\theta\sin\tilde{\alpha} \quad (17)$$

$$R_e.\delta^3\left[\left(-\frac{\partial\psi}{\partial y}.\frac{\partial}{\partial x} + \frac{\partial\psi}{\partial x}.\frac{\partial}{\partial y}\right)\frac{\partial\psi}{\partial x} - \frac{\partial^2\psi}{\partial x^2}\right] = -\frac{\partial p}{\partial y} - \delta^2\left(\delta^2\frac{\partial^3\psi}{\partial x^3} + \frac{\partial^3\psi}{\partial y^2\partial x}\right) + \frac{\delta^2}{\gamma^2}\left(\delta^4\frac{\partial^5\psi}{\partial x^5} + 2\delta^2\frac{\partial^5\psi}{\partial x^3\partial y^2} + \frac{\partial^5\psi}{\partial y^4\partial x}\right) + H^2\,\delta\,\sin\Phi\left[\left(\frac{\partial\psi}{\partial y} + 1\right)\cos\Phi + \frac{\partial\psi}{\partial x}\,\delta\sin\Phi\right] + \frac{\delta^2}{D_a}.\frac{\partial\psi}{\partial x} - \frac{R_e}{F_r}\,\delta\cos\tilde{\alpha} \quad (18)$$

$$R_e.\delta.P_r\left(\frac{\partial\psi}{\partial y}.\frac{\partial\theta}{\partial x} + \frac{\partial\theta}{\partial x} - \frac{\partial\psi}{\partial x}.\frac{\partial\theta}{\partial y}\right) = \left(\delta^2\frac{\partial^2\theta}{\partial x^2} + \frac{\partial^2\theta}{\partial y^2}\right) + B_r\left[4\delta^2\left(\frac{\partial^2\psi}{\partial x\partial y}\right)^2 + \left(\frac{\partial^2\psi}{\partial y^2} - \delta\frac{\partial^2\psi}{\partial x^2}\right)^2 + \frac{1}{\gamma^2}\left[\left(\delta^2\frac{\partial^3\psi}{\partial x^2\partial y} + \frac{\partial^3\psi}{\partial y^3}\right)^2 + \left(\delta^2\frac{\partial^3\psi}{\partial x^3} + \frac{\partial^3\psi}{\partial x\partial y^2}\right)^2\right]\right] + B_r\,H^2\left[\left(\frac{\partial\psi}{\partial y} + 1\right)\cos\Phi + \frac{\partial\psi}{\partial x}\,\delta\sin\Phi\right]^2, \quad (19)$$

under the assumption of long wavelength approximation (δ<< 1) and low Reynolds number, The eliminating pressure terms using cross differentiation from the dimensionless Equations (17-19) , one can write a single differential equation in terms of stream function as follows:

$$\frac{\partial^6\psi}{\partial y^6} - \gamma^2\frac{\partial^4\psi}{\partial y^4} + H^2\gamma^2\cos^2\Phi.\frac{\partial^2\psi}{\partial y^2} + \frac{\gamma^2}{D_a}.\frac{\partial^2\psi}{\partial y^2} = 0 \quad (20)$$

$$\frac{\partial^2\theta}{\partial y^2} + B_r\left[\left(\frac{\partial^2\psi}{\partial y^2}\right)^2 + \frac{1}{\gamma^2}\left(\frac{\partial^3\psi}{\partial y^3}\right)^2\right] + B_r\,H^2\cos^2\Phi\left(\frac{\partial\psi}{\partial y}\right)^2 = 0 \quad (21)$$

The dimensionless boundary conditions in the wave frame are [9]:

$$\frac{\partial\psi}{\partial y} + \beta\frac{\partial^2\psi}{\partial y^2} = -1 \quad on\ y = h_1$$

$$\frac{\partial \psi}{\partial y} - \beta \frac{\partial^2 \psi}{\partial y^2} = -1 \quad on\ y = h_2$$
$$\psi = \frac{F}{2} \qquad , \theta = 0 \ \ on \ \ y = h_1 \tag{22}$$
$$\psi = -\frac{F}{2} \qquad , \theta = 1 \ \ on \ \ y = h_2$$
$$\frac{\partial^3 \psi}{\partial y^3} = 0 \ on\ y = h_1 \ and \ y = h_2$$

As a result of solving equations (20) and (21), the associated boundary conditions (22) are satisfied.

$$\psi = B_5 + yB_6 + 2\left(-\frac{e^{-A_1 y}B_1}{A_3} - \frac{e^{A_1 y}B_2}{A_3} + \frac{e^{-A_2 y}B_3}{A_4} + \frac{e^{A_2 y}B_4}{A_4}\right) \tag{23}$$

$$\theta = C_1 + yC_2 + \frac{1}{2\gamma^2 A_3^3 A_4^3}(2y^2\mathcal{H}^2\gamma^2 Cos[2\Phi]A_1^2A_3A_4^3B_1B_2B_r + 4y^2\mathcal{H}^2\gamma^2 Cos[2\Phi]^2A_1^2A_3A_4^3B_1B_2B_r + 2y^2\mathcal{H}^2\gamma^2 Cos[2\Phi]Cos[4\Phi]A_1^2A_3A_4^3B_1B_2B_r - 2iy^2\mathcal{H}^2\gamma^2 Sin[2\Phi]A_1^2A_3A_4^3B_1B_2B_r - 2iy^2\mathcal{H}^2\gamma^2 Cos[4\Phi]Sin[2\Phi]A_1^2A_3A_4^3B_1B_2B_r + 4y^2\mathcal{H}^2\gamma^2 Sin[2\Phi]^2A_1^2A_3A_4^3B_1B_2B_r + 2iy^2\mathcal{H}^2\gamma^2 Cos[2\Phi]Sin[4\Phi]A_1^2A_3A_4^3B_1B_2B_r + 2y^2\mathcal{H}^2\gamma^2 Sin[2\Phi]Sin[4\Phi]A_1^2A_3A_4^3B_1B_2B_r) \ldots \tag{24}$$

The velocity can be written as:

$$u_\circ = 2\left(\frac{e^{-yA_1}A_1B_1}{A_3} - \frac{e^{yA_1}A_1B_2}{A_3} - \frac{e^{-yA_2}A_2B_3}{A_4} + \frac{e^{yA_2}A_2B_4}{A_4}\right) + B_6 \tag{25}$$

Where $(B_1,\ B_2,\ B_3,\ B_4,\ B_5,\ B_6,\ C_1,\ C_2)$ are constant, $A_1 = \frac{\sqrt{\gamma^2 - \sqrt{\gamma^2(-2\mathcal{H}^2+\gamma^2-2\mathcal{H}^2\mathrm{Cos}[2\Phi]-\frac{4}{D_a})}}}{\sqrt{2}}$, $A_2 = \frac{\sqrt{\gamma^2 + \sqrt{\gamma^2(-2\mathcal{H}^2+\gamma^2-2\mathcal{H}^2 Cos[2\Phi]-\frac{4}{D_a})}}}{\sqrt{2}}$, $A_3 = -\gamma^2 + \sqrt{\gamma^2(-2\mathcal{H}^2+\gamma^2-2\mathcal{H}^2 Cos[2\Phi]-\frac{4}{D_a})}$ and $A_4 = \gamma^2 + \sqrt{\gamma^2(-2\mathcal{H}^2+\gamma^2-2\mathcal{H}^2\mathrm{Cos}[2\Phi]-\frac{4}{D_a})}$

The axial pressure gradient can be calculated once we've identified the stream function.

$$\frac{\partial p}{\partial x} = \frac{\partial^3 \psi}{\partial y^3} - \frac{1}{\gamma^2}.\frac{\partial^5 \psi}{\partial y^5} - H^2\, cos^2\, \Phi\left[\left(\frac{\partial \psi}{\partial y} + 1\right)\right] - \frac{1}{D_a}\left(\frac{\partial \psi}{\partial y} + 1\right) + \frac{R_e}{F_r}\sin\tilde{\alpha} + \mathrm{G}_r\theta\ \sin\tilde{\alpha} \tag{26}$$

$$\frac{\partial p}{\partial y} = 0 \tag{27}$$

In non-dimensional form, the pressure rise per wavelength $\Delta p_\circ$ is defined as

$$\Delta p_\circ = \int_0^1 \frac{\partial p}{\partial x}\mathrm{dx} \tag{28}$$

The heat transfer coefficient (M) is defined at the top and bottom wall of the channel as

$$\mathrm{Mh}_1 = \frac{\partial h_1}{\partial x}.\frac{\partial \theta}{\partial y} \quad \text{and} \quad \mathrm{Mh}_2 = \frac{\partial h_2}{\partial x}.\frac{\partial \theta}{\partial y} \tag{29}$$

3.Volumetric flow rate

In the laboratory frame, the volumetric flow rate is equal to

$$Q = \int_{\overline{h_2}}^{\overline{h_1}} \overline{\mathrm{U}}\ (\overline{\mathrm{X}}\ , \overline{\mathrm{Y}}, \overline{\mathrm{t}})\mathrm{d}\overline{\mathrm{Y}} \tag{30}$$

where $\overline{h_1}$ and $\overline{h_2}$ are functions of $\bar{X}$ and $\bar{t}$.
In the wave frame, the volumetric flow rate is calculated:

$$q = \int_{\overline{h_2}}^{\overline{h_1}} \grave{u}(\grave{x}, \grave{y}) d\grave{y} . \quad (31)$$

The relationship between Q and q can is calculated as follows:

$$Q = q + c\left(\overline{h_1} - \overline{h_2}\right) . \quad (32)$$

Time-mean flow over a span of time T^* fixed in place $\bar{X}$ as

$$Q^* = \frac{1}{T^*}\int_0^{T^*} Q dt . \quad (33)$$

Using equation (32) in equation (33) the flow rate Q^* has the From

$$Q^* = \frac{1}{T^*}\int_0^{T^*} q dt + c\left(\overline{h_1} - \overline{h_2}\right)$$

$$= q + cd_1 + cd_2 + 2cx\lambda \tan\tilde{\alpha} + ca_1 \cos(2\pi x) + ca_2 \cos(2\pi x + \phi). \quad (34)$$

The non-dimensional of equation (31) is provided by

$$\vartheta = F + 1 + d + 2kx + a\cos(2\pi x) + b\cos(2\pi x + \phi) \quad (35)$$

where $\vartheta = \frac{Q^*}{cd_1}$ and $F = \frac{q}{cd_1}$ the expression in the form

$$F = \int_{h_2}^{h_1} \frac{\partial \psi}{\partial y} dy = \psi(h_1) - \psi(h_2) . \quad (36)$$

4. Numerical Results and Discussion

The analysis of "$u_\circ$" axial velocity, "M" heat transfer coefficient, "θ" temperature, "δP" pressure gradient, "$\Delta p_\circ$" pressure rise, and "ψ" stream function are determined in this section.

The "MATHEMATICA" program was used to calculate the numerical values corresponding to the above-mentioned analytical formulae.

4.1 . The distribution of velocity

This part is to examine the impact of the axial velocity ($u_\circ$) variation across the channel at various parameters. Shows a noticeable rise in velocity in the center regions of the channel phase difference ϕ, whereas the axial velocity falls at the channel wall's boundary, as seen in Figure 2(a). Figure 2(b) shows that when Darcy number "D_a" increases, the axial velocity also increases in the middle area, whereas the axial velocity falls at the channel wall's boundary. Since less resistance to fluid flow is provided by a more permeable porous medium, this finding is supported by the laws of physics. It is shown in Figure 2(c) that with an increasing Hartmann number H, axial velocity reduces in the center portion of the channel. The Lorentz force is responsible for this finding. As seen in Figure 2(d), increasing couple stress parameter γ reduces the axial velocity in the middle portion of the channel. The flattening of velocity profiles occurs as particle size in the fluid increases, resulting in a drop in velocity. To ensure the conservation of mass. Figure 2 (e and f) illustrates that as slip parameterβ and k are increased, the axial velocity drops in the center regions of the channel. In Figure 2(g), it is shown that the velocity of the fluid increases in the middle area, whereas the axial velocity reduces at the channel wall's boundary $y \in [-1,1]$ as the channel the inclination of the magnetic field angle Φ increases.

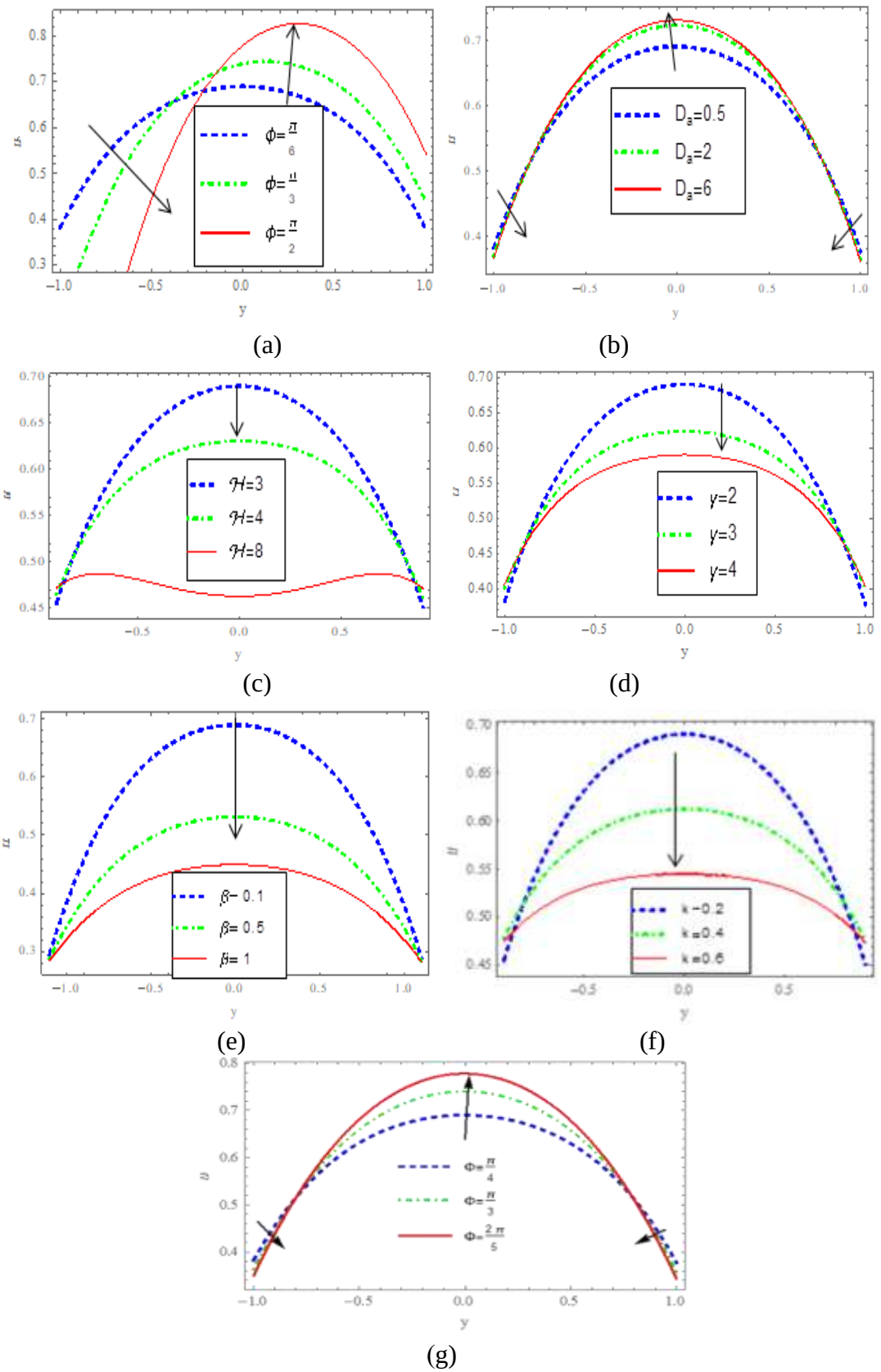

Figure 2: Variation the axial velocity "$u_\circ$" with different perimeters$\{D_a = 0.5, \mathcal{H} = 3, \gamma = 2, a = 0.6, b = 0.7, d = 1, \beta = 0.1, \phi = \frac{\pi}{6}, F = 1, k = 0.2, \Phi = \frac{\pi}{4}, x = 1\}$

4.2 . Pumping characteristics

In this subsection, we will analyze the pressure through the channel.

4.2.1. pressure gradient"δP"

Each of the figures in this section illustrates the pressure gradient along the axial axis of fluctuation along the channel at one wavelength $x \in [0,1]$. Figures like this show that flow is restricted in the narrowing portion of channel $x \in [0.2,0.6]$. As a result, a larger pressure gradient is needed to achieve a normal flow. Because of the smaller pressure gradient in the larger area of the channel $x \in [0,0.2] \cup [0.6,1]$, fluid may pass readily. Figure 3(a) shows that when the *H*artmann number$H$ raises, the pressure gradient also increases in size. This graphic shows that greater pressure is required to move some volume of fluid through the narrower region of the channel when the magnetic field is strong. When looking at channel parameters such as the inclination$\widetilde{\alpha}$ of the channel, the magnetic field inclination angle Φ, Grashof numbers G_r, the slip parameterβ, Darcy number "D_a", Reynolds number"R_e", Couple stress "γ", temperature "θ", non-uniformity "k" and the phase difference"ϕ"as depicted in Figures 3(b-z), the pattern is the opposite. Because of the inclination, less pressure is needed to move liquids.

4.2.2. pressure rise"$\Delta p_\circ$"

Figure 4(a-z) shows how the pressure rise in the wave frame varies with the rate of volumetric flow for various values of the rate of volumetric flow. The connection between pressure rise and rate of volumetric flow for each wavelength is seen to be linear. The whole region is considered into five parts (1) the peristaltic pumping region where$(\Delta p_\circ > 0, F > 0)$ (2) when $(\Delta p_\circ > 0, F < 0)$, then it is a retrograde pumping region (3) augmented pumping (co-pumping) region where $(\Delta p_\circ < 0, F > 0)$ (4) There is a co-pumping region where $(\Delta p_\circ < 0, F < 0)$ (5) $(\Delta p_\circ = 0)$corresponds to the free pumping region.

Figure4 (a) shows the impact of Hartmann number "H" on $\Delta p_\circ$. It has been noticed in the retrograde pumping region. The pumping rate increases as Hartmann number "H" increases. Co-pumping reduces when in this region and increases in "H". Volumetric flow rate and pressure increase $\Delta p_\circ$, shown to be linearly related in Figures 4 (b-e) for a variety of Grashof numbers "G_r" , "R_e"," $\tilde{\alpha}$" and "θ ". We observed that the results rise in an increase in retrograde pumping rate and when the pressure rise, the augmented pumping (co-pumping) region is increasing. Figure 4 (f-h) shows that with an increase in "β", "γ" and " D_a", the pumping rate decreases in the region of retrograde pumping, while in the augmented pumping region found to increase. Figure 4 (i)shows an impact of channel non-uniform parameter "k"on $\Delta p_\circ$. It is observed that in a retrograde pumping region and a free pumping region $(\Delta p_\circ = 0)$, the pumping rate decreases with an increase in "k". Figure 4 (j) depicts the effect of "ϕ" on $\Delta p_\circ$. It is observed that in a retrograde pumping region and a free pumping region $(\Delta p_\circ = 0)$, the pumping rate increases with an increase in"ϕ". We noted that a rise in the inclination mechanic field angle "Φ" results in a decrease in the retrograde pumping rate and augmented pumping (co-pumping) region a rise in the pressure rise in Figure 4 (z) .

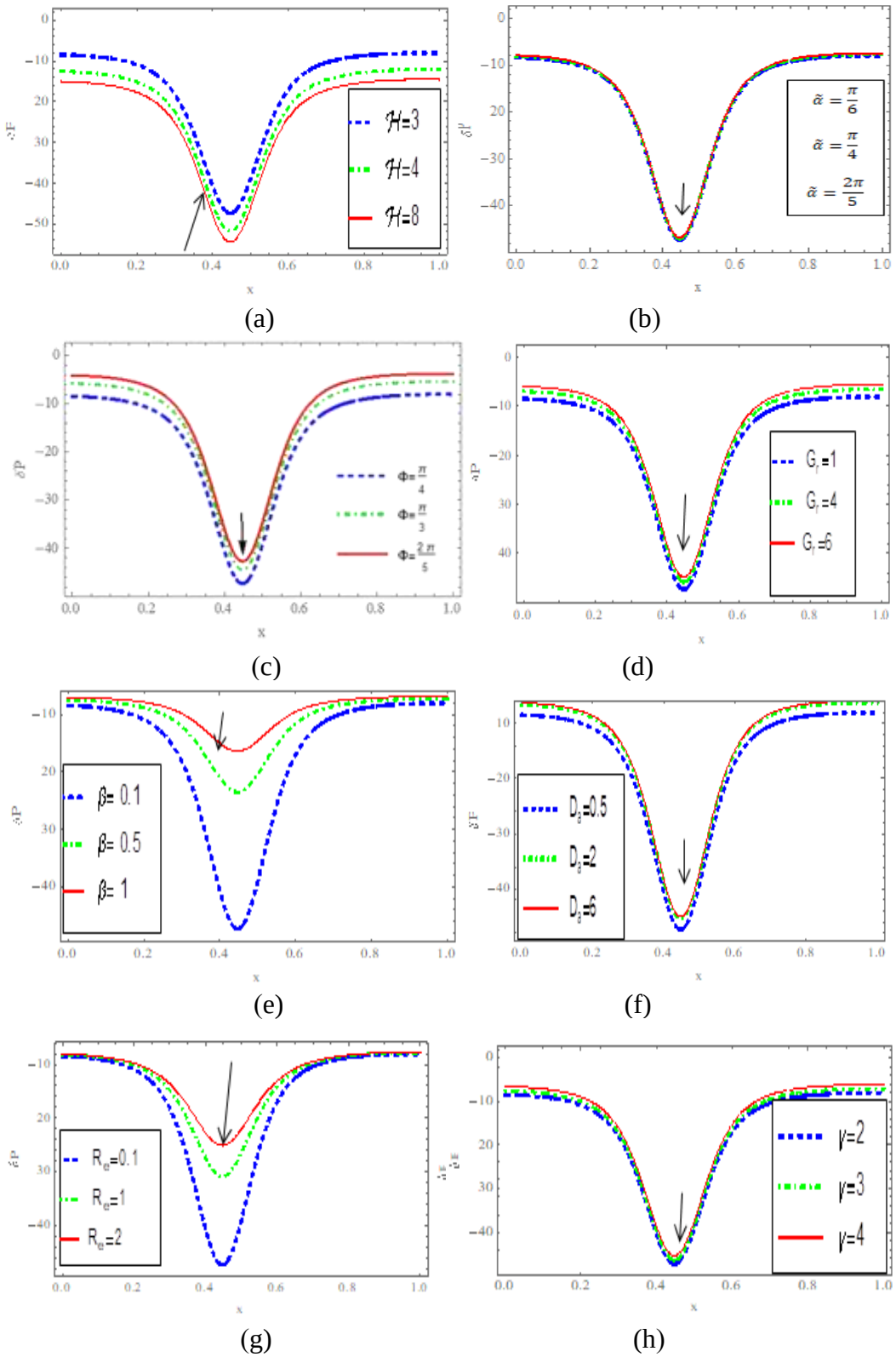
H=3
H=4
H=8
α̃ = π/6
α̃ = π/4
α̃ = 2π/5
Φ= π/4
Φ= π/3
Φ= 2π/5
G_r=1
G_r=4
G_r=6
β= 0.1
β= 0.5
β= 1
D_a=0.5
D_a=2
D_a=6
R_e=0.1
R_e=1
R_e=2
γ=2
γ=3
γ=4
x
(a)
(b)
(c)
(d)
(e)
(f)
(g)
(h)

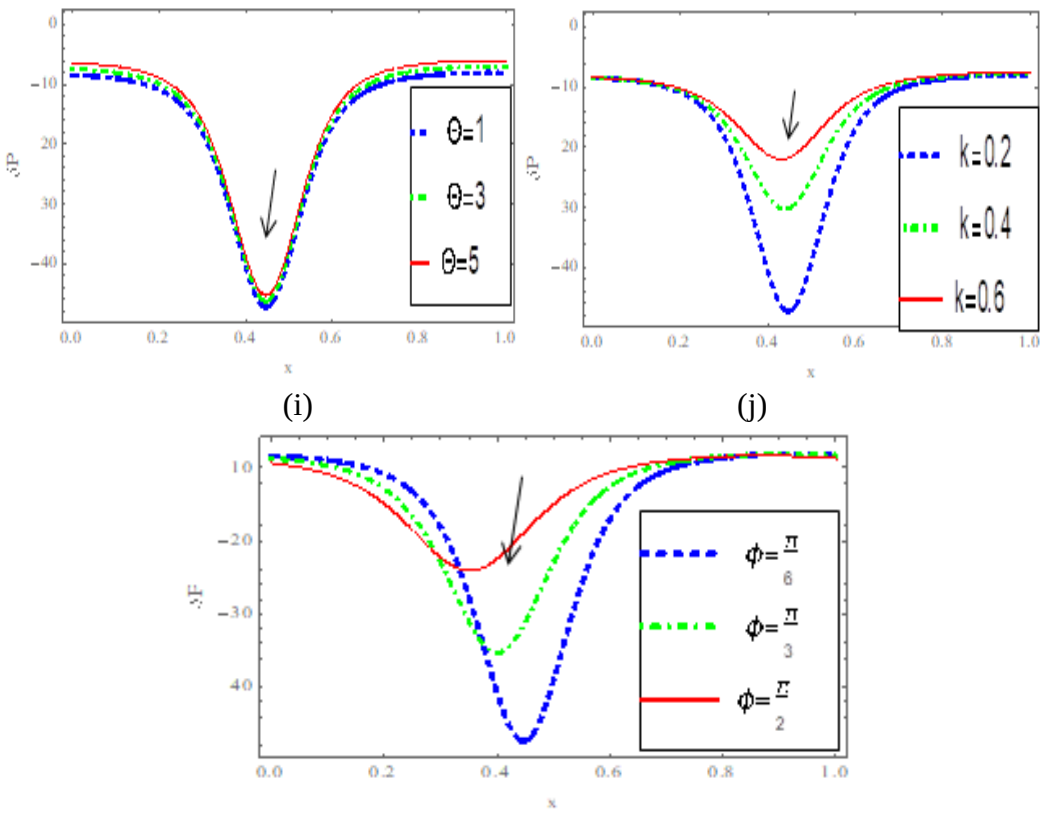

(i) (j)

(z)

Figure 3: Variation the pressure gradient" δP" with different perimeters$\{D_a = 0.5, \mathcal{H} = 3, \gamma = 2, a = 0.6, b = 0.7, d = 1, \beta = 0.1, \phi = \frac{\pi}{6}, F = 0.1, k = 0.2, F_r = 0.5, \tilde{\alpha} = \frac{\pi}{6}, R_e = 0.1, G_r = 1, \Phi = \frac{\pi}{4}, \Theta = 1, y = 1\}$

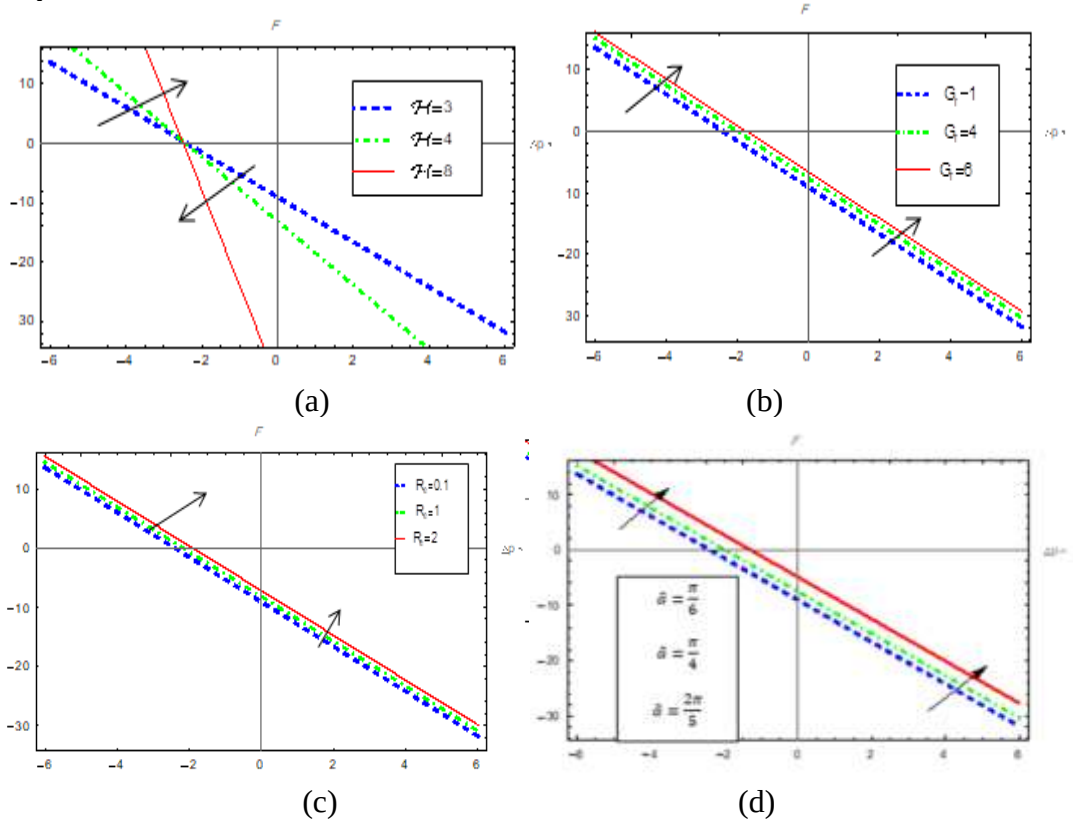

(a) (b)

(c) (d)

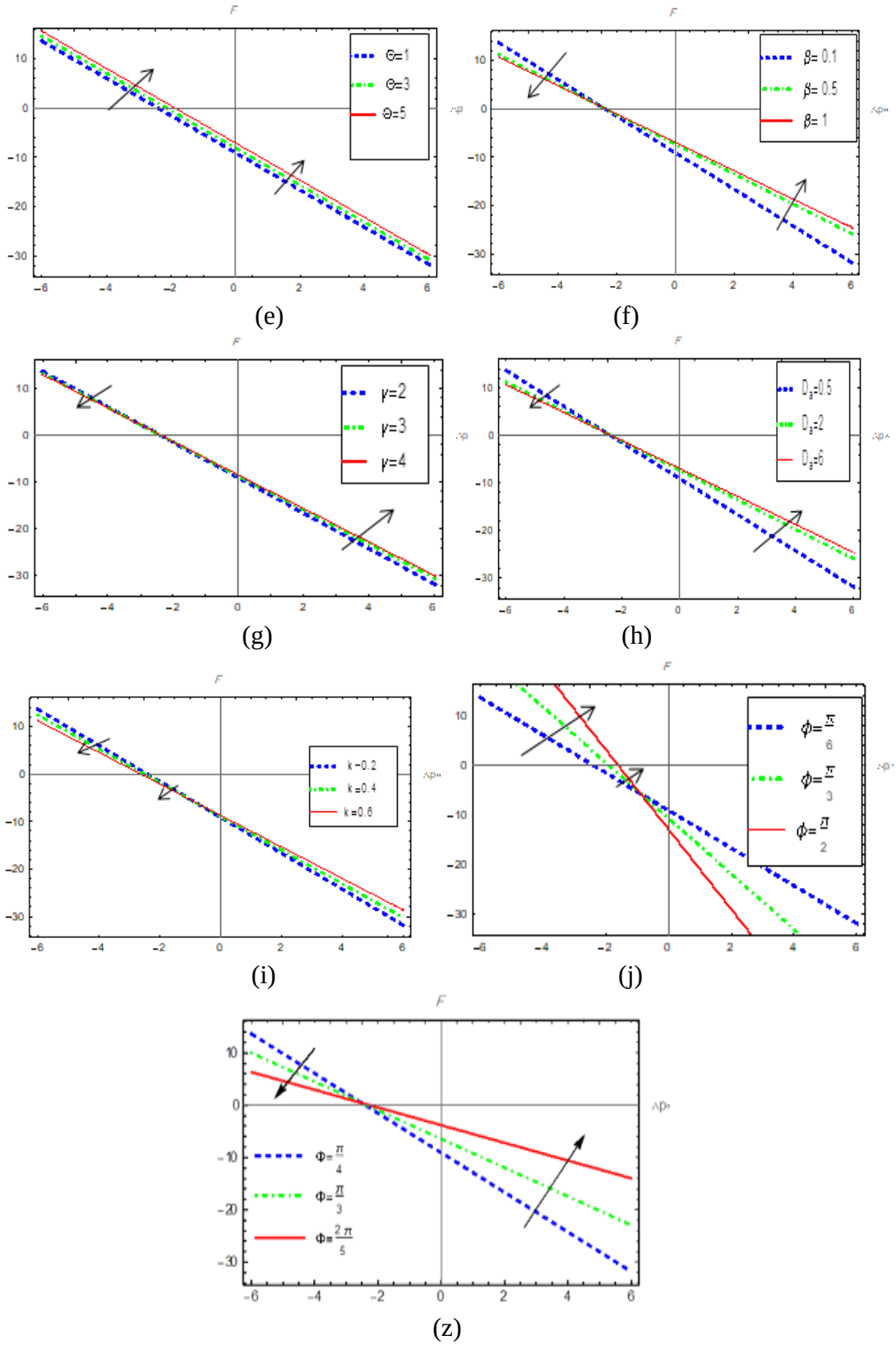

Figure 4: Variation pressure rise"$\Delta p_\circ$"with different perimeters$\{D_a = 0.5, \mathcal{H} = 3, \gamma = 2, a = 0.6, b = 0.7, d = 1, \beta = 0.1, \phi = \frac{\pi}{6}, k = 0.2, F_r = 0.5, \tilde{\alpha} = \frac{\pi}{6}, R_e = 0.1, G_r = 1, \Phi = \frac{\pi}{4}, \Theta = 1, y = 1\}$

4.3 . Heat transfer coefficient (M)

A number of parameters have been taken into account in this section to see how they affect the heat transfer coefficient (M). In relevant settings, the oscillatory behavior of the heat transfer coefficient (Mh_1) on the top wall and of the heat transfer coefficient (Mh_2) at the bottom wall may be seen due to peristaltic waves contracting and expanding along the channel walls. As it is observed from Figure 5 (a1-c1), the heat transfer coefficient (Mh_1) increases with the increase of "γ", "H" and "B_r" . It is shown in Figure 5 (d 1-g1) , the heat transfer coefficient(Mh_1) reduces with the rise of "Φ" ," D_a", "β" and"ϕ". As can be seen in Figure 6(a2-g2), there is a similarity in the results between the heat transfer coefficient (Mh_1) on the top wall and the heat transfer coefficient (Mh_2) on the bottom wall.

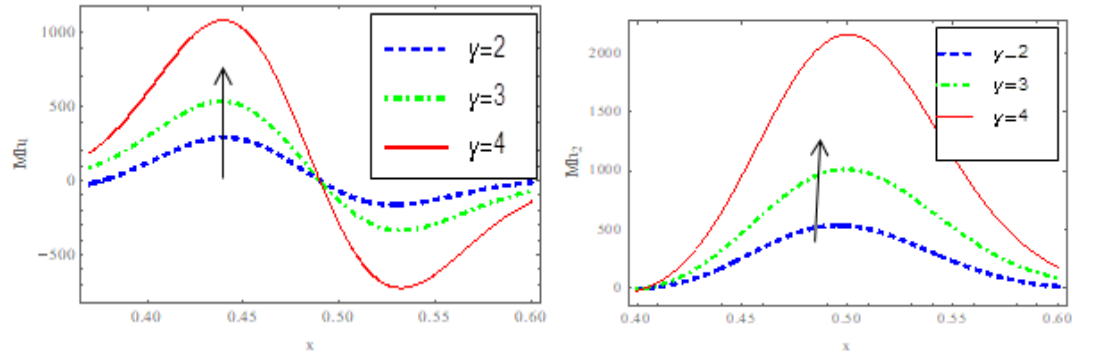

(a1) (a2)

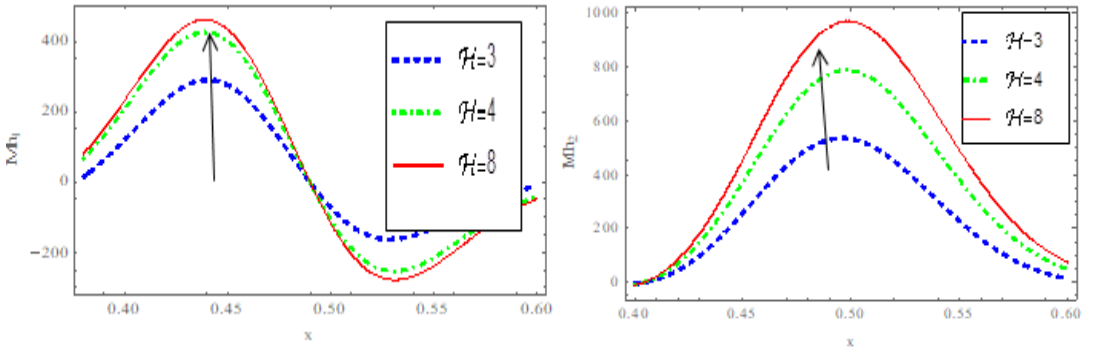

(b1) (b2)

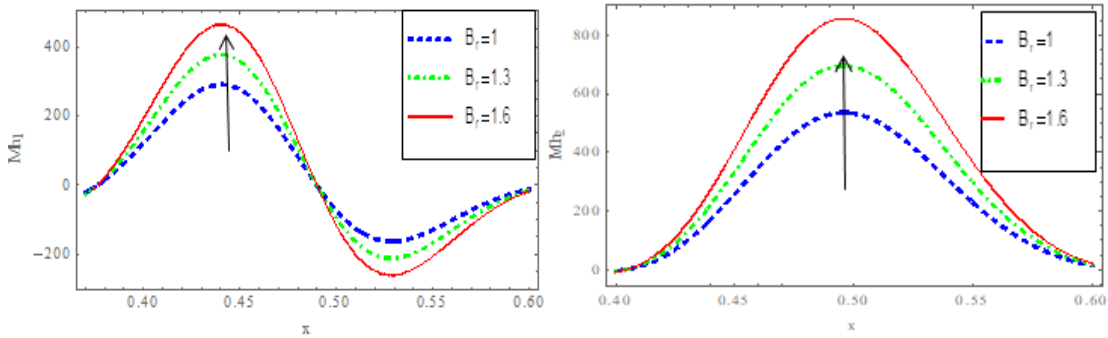

(c1) (c2)

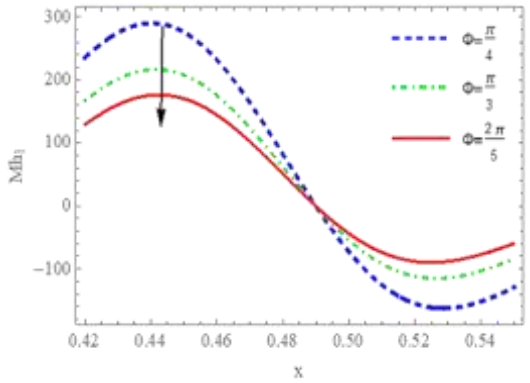

(d1)

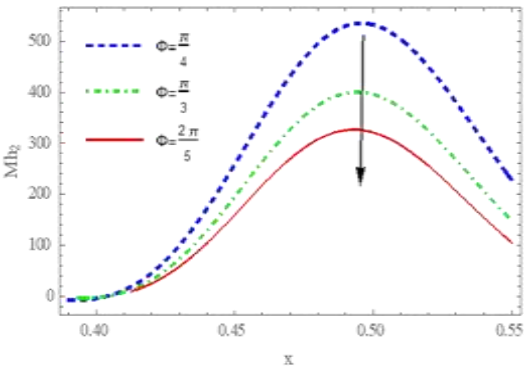

(d2)

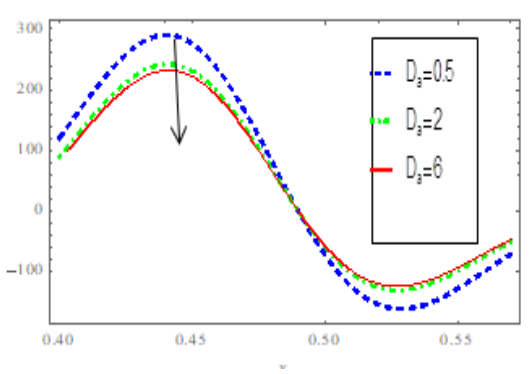

(e1)

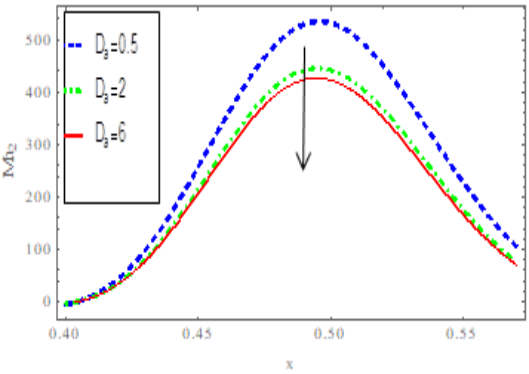

(e2)

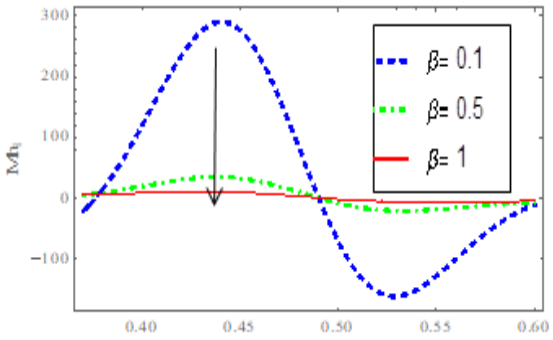

(f1)

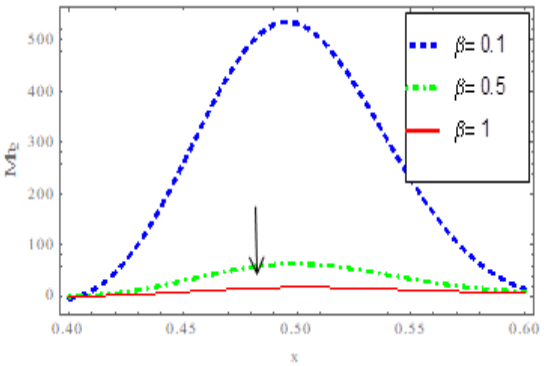

(f2)

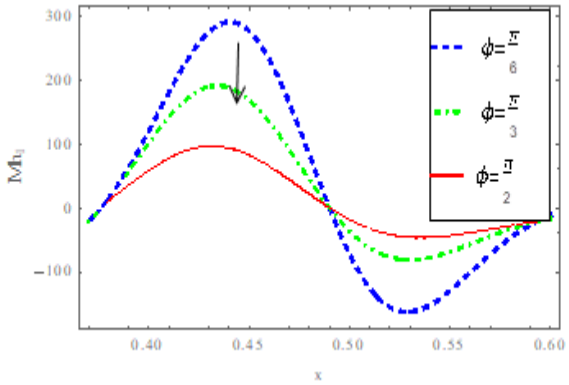

(g1)

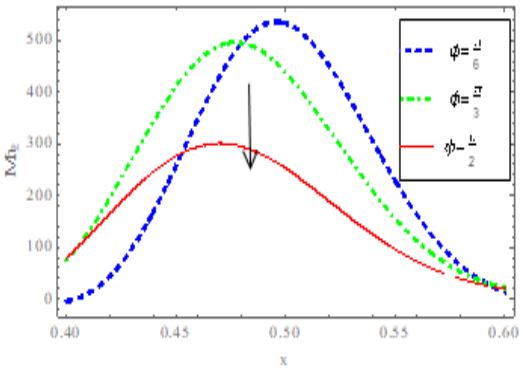

(g2)

Figure 5: Heat transfer coefficient(Mh_1) for different values of parameters

Figure 6: Heat transfer coefficient(Mh_2) for different values of parameters

4.4. The distribution of temperature "θ"

This paragraph focuses on the effect of parameters on the fluid temperature profile, which is examined at the fixed value of x = 1. parabolic temperature profile with a higher graph near its center. If the viscosity of a flowing fluid is high, it will convert kinetic energy from its movement into internal energy, which heats the fluid. This is a rather clear fact. Figure 7 (a-d) shows that the temperature decreases as "β", "γ",ϕ and "Φ" increase. As parameter values "D_a", "H", "k"and "B_r"increase, the temperature in the channel's center is increased. This is shown in Figure 7 (e-h). The increase in temperature is accompanied by "B_r". $Brinkman$ number "B_r"values cause increasing flow resistance due to shear, which causes increased heat generation due to the viscous dissipation influence and raises the fluid's temperature.

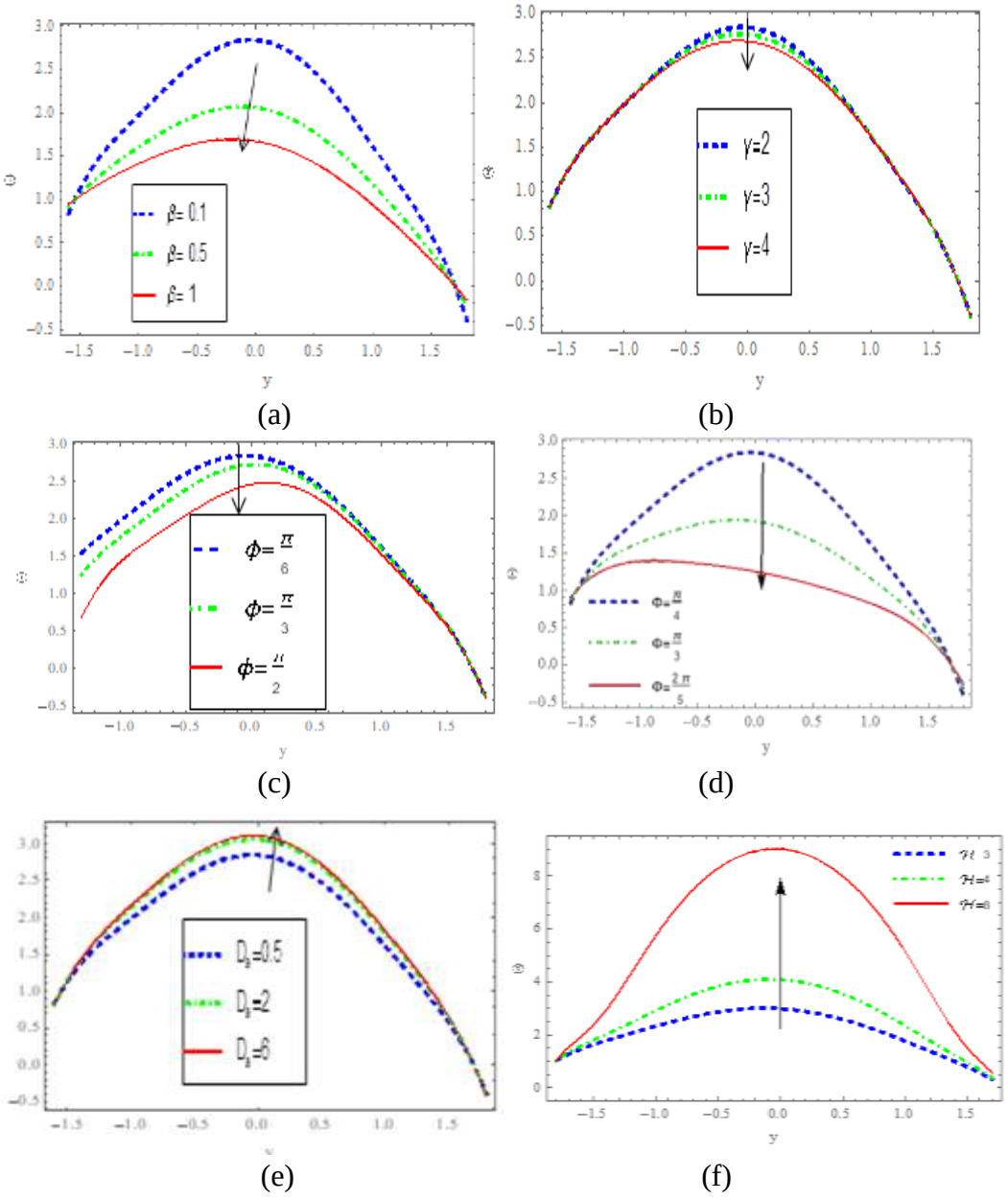

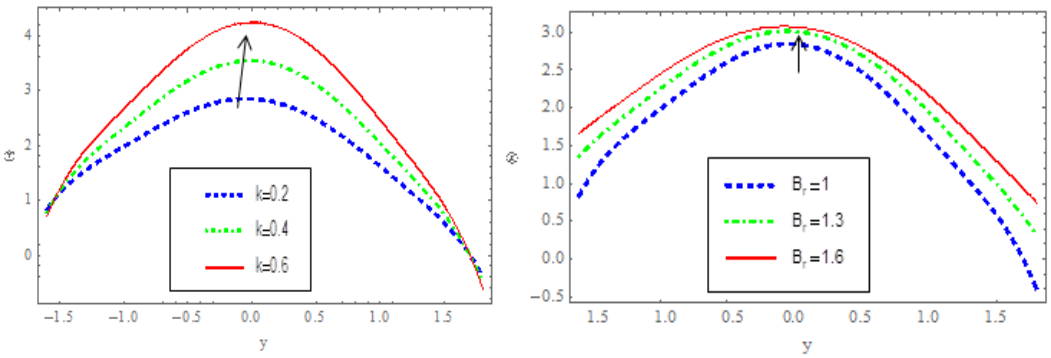

(g) (h)

Figure 7: Variation temperature θwith different perimeters$\{D_a = 0.5, \mathcal{H} = 3, \gamma = 2, a = 0.6, b = 0.7, d = 1, \beta = 0.1, \phi = \frac{\pi}{6}, F = 1, k = 0.2, B_r = 1, \Phi \to \frac{\pi}{4}, x = 1\}$

4.5. The trapping phenomena

In order to explain the trapping phenomena, The formation of a circulating bolus of fluid, which is a closed streamline region, at the speed of the wave. There will be points in the wave frame where the fluid's velocity is zero due to the trapping phenomenon. The volumetric flow rate via a line linking any two places is computed by taking into account the difference in stream function values at the two sites in question. Images 8–14 indicate that bolus formation occurs on both sides of the central line in the extended region. Bigger and larger volumes of the trapped bolus can be extracted from the system by raising the strength of the magnetic field in Figure 8 (a, b and c), as magnetic field inclination angle "Φ". In Figures 9 and 10 (a, b, and c), as phase parameter "ϕ" and slip parameter "β" change, the variation in streamlines will also change. According to our research, we found that bolus sizes decrease as phase parameter" ϕ" and slip parameter "β" increase. In Figure 11 (a, b, and c), it is easy to see how streamlines changes the bolus size increases as the Darcy number " D_a", increases. These Figures 12and13 (a, b, and c), demonstrate how the increase in the Hartman number " H'', and couple stress "γ", the incidence of trapped bolus diminishes in size and vanishes in the direction of downstream. Another effect that may help protect red blood cells and other elements is the tendency to reduce bolus volume. Graphing the non-uniformity coefficient of the asymmetric channel as shown in Figure 14 (a, b, and c). When the non-uniform parameter "k" is raised, the trapped bolus decrease in size and migrates downstream. these figures demonstrate that the wall draws fluid in the wider section of the channel, but that fluid is pushed away from the wall in the narrower section.

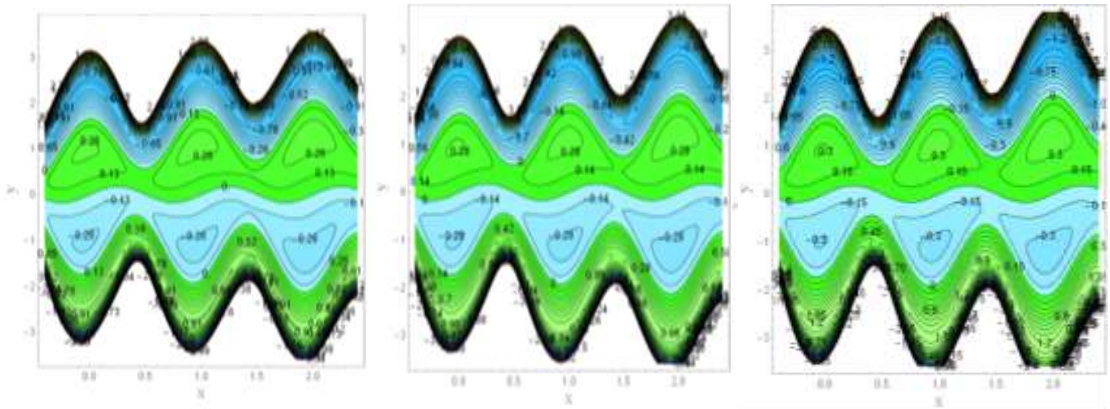

(a) (b) (c)

Figure 8: Distribution of streamlines " ψ" for (a) "Φ" =π/4 (b) "Φ"=π/3 (c) "Φ" = 2π/5

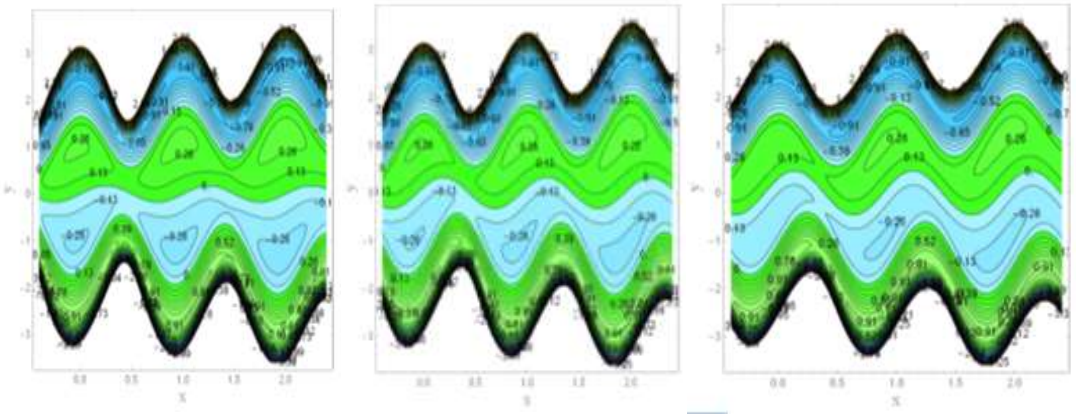

(a) (b) (c)

Figure 9: Distribution of streamlines " ψ" for (a) " ϕ" = π/6 (b) " ϕ"= π/3 (c) " ϕ"= π/2

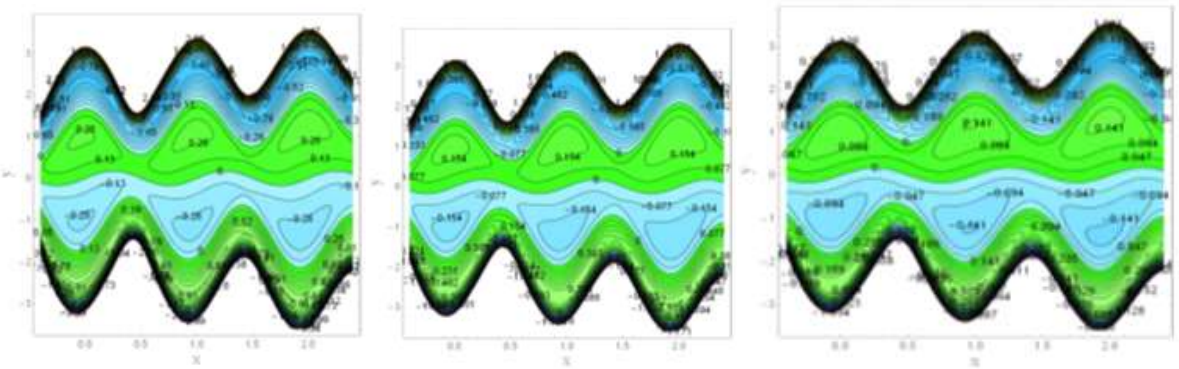

(a) (b) (c)

Figure 10 : Distribution of streamlines " ψ" for (a) "β" =0.1 (b) "β" = 0.5 (c) "β"=1

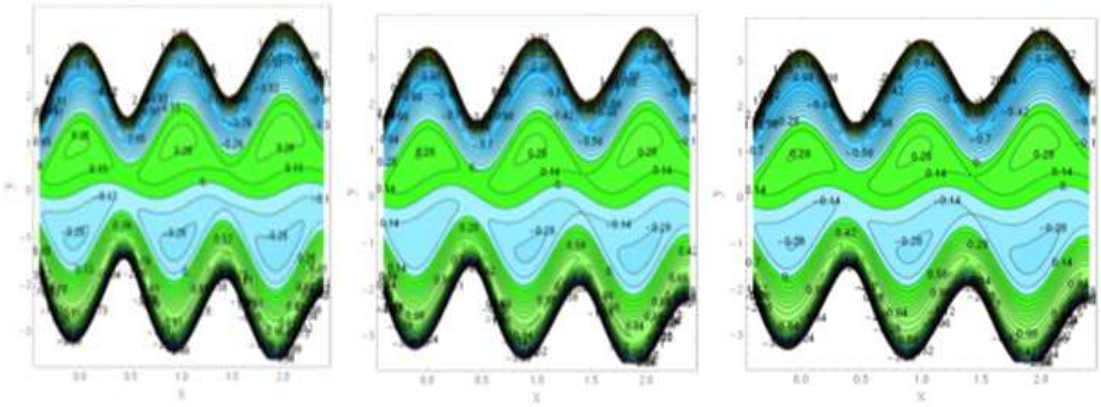

(a) (b) (c)

Figure 11: Distribution of streamlines " ψ for (a) " D_a" =0.5 (b) " D_a" =2 (c) " D_a"=6

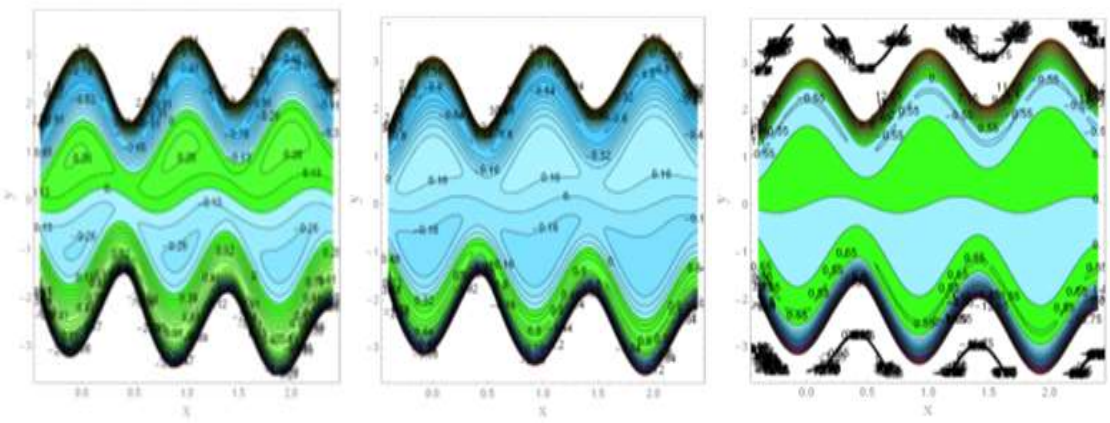

(a) (b) (c)

Figure 12: Distribution of streamlines " ψ" for (a) " H'' =3 (b) " H''= 4 (c) " H''=8

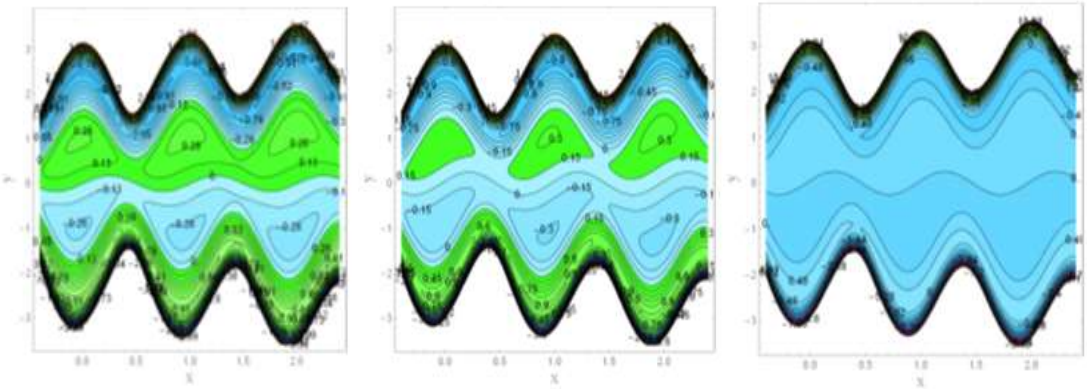

(a) (b) (c)

Figure 13: Distribution of streamlines " ψ" for (a) "γ" =2 (b) "γ" = 3 (c) "γ"=4

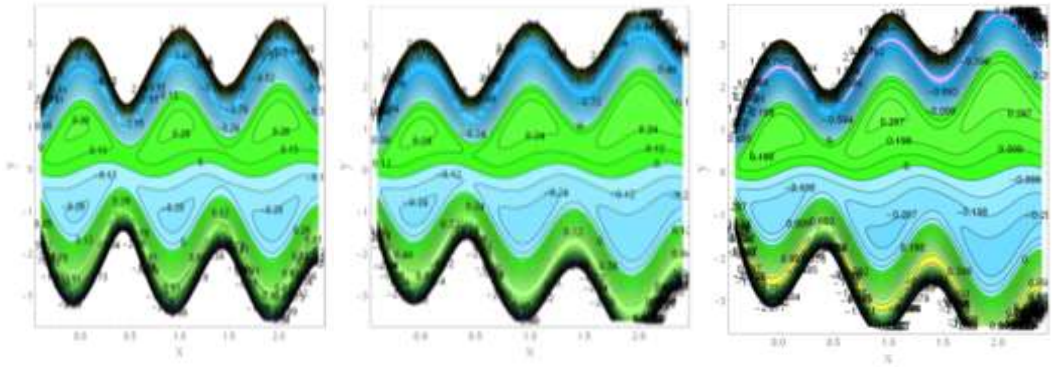

(a) (b) (c)

Figure 14: Distribution of streamlines " ψ" for (a) "k" =0.2 (b) "k" = 0.4 (c) "k"=0.6

5. Conclusions

In this paper, we use incline magnetohydrodynamics to investigate the effects of heat transfer and couple stress fluid as they move via an inclined asymmetric channel and porous medium under low Reynolds approximations and long-wavelength assumptions in the transport of bodily fluids by the use of non-Newtonian fluid models. Analytically, using a straightforward mathematical formula. this investigation focused on studying the distribution of velocity, the

pumping characteristics, the distribution of temperature, the trapping phenomena, and the heat transfer coefficient.

1. There is an increase in axial velocity "$u_\circ$" in the central region when an increase in the phase difference"ϕ", the inclination magnetic field angle "Φ"and the Darcy number " D_a", but there is a decrease in velocity at the boundary of the channel wall.
2. There is an decrease in axial velocity "$u_\circ$" in the central region when increasing the couple stress parameter "γ", Hartmann number " H'', slip parameter "β", channel non-uniform parameter "k".
3. There is an increase in "δP " pressure gradient when an increase in the Hartmann number " H'', while a decreasing with the rising values of slip parameter "β", the inclination magnetic field angle "Φ", the inclination "$\widetilde{\alpha}$" of the channel, Grashof number "G_r", Darcy number " D_a", the couple stress parameter "γ", the phase difference "ϕ", non-uniform parameter "k", Reynolds number "R_e" and temperature "θ " .
4. The connection between pressure rise "$\Delta p_\circ$"and volumetric flow rate for each wavelength is seen to be linear.
5. In retrograde pumping, increases"$\Delta p_\circ$" pressure rise with the increasing values "G_r","R_e", "H'', "θ ", "$\widetilde{\alpha}$" and "ϕ", whereas it decreases with the rising values "D_a" , "γ", "Φ", "β" and "k''.
6. The temperature "θ" rises when "k", "D_a", " H'' and Brinkman number"B_r" all go up. It goes to decrease when the slip parameter "β", the inclination magnetic field angle "Φ" ,couple-stress parameter"γ", and phase difference "ϕ" all go up.
7. The heat transfer coefficient(Mh_1) at the upper wall increases with the increase of the Brinkman number "B_r" , " H'' and "γ", the heat transfer coefficient (Mh_1) decreases with the increase of "Φ", "β", "D_a" and"ϕ". There is a similarity in the results between the heat transfer coefficient (Mh_1) on the top wall and the heat transfer coefficient (Mh_2) on the bottom wall.
8. When values are increased "H'' and "γ", it is possible to eliminate trapped bolus. slip parameter "β", "k" and "ϕ" have a decreasing impact on the bolus size, whereas it increases the bolus size with the increasing values of "Φ" and Darcy number "D_a".

References

[1] T. Hayat, M. Khan and S. Asghar, "Peristaltic transport of a third order fluid under the effect of a magnetic field, "*Appl Math Comput*, vol. 53, pp. 1074-1087, 2007.

[2] M.M. Bhatti, M. Ali Abbas and M.M. Rashidi, "Combine effects of Magnetohydrodynamics (MHD) and partial slip on peristaltic Blood flow of Ree–Eyring fluid with wall properties," *Engineering Science and Technology, an International Journal*, vol.19, no.3, pp. 1497-1502, 2016.

[3] S. Rahman, T. Hayat and H. Alsulami, "Some new regularity criterion for MHD three-dimensional flow," *Kuwait Journal of Science*, vol.44, no. 4, pp. 28-48, 2017.

[4] V.K. Stokes, "Couple stress in fluid. *Phys. Fluid*," *Phys. Fluid*, vol.9, pp. 1709-1715, 1966.

[5] Kh. S. Mekheimer, "Effect of induced magnetic field on peristaltic flow of a couple stress fluid," *Physics Letters A*, vol.372, pp. 4271-4278, 2008.

[6] H. Abdulhussain and A. M. Abdulhadi, "Peristaltic Transport of Couple Stress Fluid through an Inclined Asymmetric and Non-Uniform Channel with Porous Medium," *International Journal of Science and Research (IJSR)*, vol.7, no. 2, pp.7-16, 2018.

[7] W. M. Hasona, A.A. El-Shekhipy and M.G. Ibrahim, "Combined effects of magnetohydrodynamic and temperature dependent viscosity on peristaltic flow of Jeffrey nanofluid through a porous medium: Applications to oil refinement ," *International Journal of Heat and Mass Transfer*, vol.126, pp.700–714, 2018.

[8] M. M. Bhatti, A. Zeeshan, M. Aleem Asif, R. Ellahi and Sadiq M. Sait, "Non-uniform pumping flow model for the couple stress particle-fluid under magnetic effects," *Chemical Engineering Communications*, DOI: 10.1080/00986445.2021.1940156, 2021.

[9] G.C. Shit and N.K. Ranjit, "Role of slip velocity on peristaltic transport of couple stress fluid through an asymmetric non-uniform channel: Application to digestive system," *Journal of Molecular Liquids*, vol .221, pp. 305-315, 2016.

[10] M. R. Salman and A. M. Abdulhadi, "Influence of heat and mass transfer on inclined (MHD) peristaltic of pseudoplastic nanofluid through the porous medium with couple stress in an inclined asymmetric channel," *Journal of Physics*: *Conference Series* 1032 012043, 2018.

[11] K. Ramesh, "Influence of heat and mass transfer on peristaltic flow of a couple stress fluid through porous medium in the presence of inclined magnetic field in an inclined asymmetric channel," *Journal of Molecular Liquids*, vol. 219, pp. 256-271, 2016.

[12] T. Hayat, A. Riaz, A. Tanveer and A. Alsaedi, " Peristaltic transport of tangent hyperbolic fluid with variable viscosity, " *Thermal Science and Engineering Progress*, vol. 6, pp. 217-225, 2018.

[13] M. R. Salman and H. A. Ali, "Approximate Treatment for The MHD Peristaltic Transport of Jeffrey Fluid in Inclined Tapered Asymmetric Channel with Effects of Heat Transfer and Porous Medium," *Iraqi Journal of Science*, vol.61, no.12 , pp. 3342-3354, 2020.